Low Cost, Flexible, Room Temperature Gas Sensor: Polypyrrole-Modified Laser-Induced Graphene for Ammonia Detection

José Carlos Santos-Ceballos, Foad Salehnia, Alfonso Romero, Xavier Vilanova, and Eduard Llobet, *Senior Member, IEEE*

***Abstract*—The electrochemical synthesis of polypyrrole (PPy) on laser-induced graphene (LIG) electrodes is investigated in this study, along with the gas-sensing applications of these modified laser-tailored materials. A simple and scalable method for the low-cost, large-scale production of PPy@LIG nanocomposites (PPy@LIG NCs) is proposed. This nanocomposite is subsequently applied to design chemoresistive flexible gas sensors to detect ammonia (NH_3) levels at room temperature. Following a brief gas exposure, PPy@LIG NCs sensors demonstrate changes in resistance with a sensitivity 14 times higher than that of pure LIG. Moreover, excellent repeatability in results and a low detection limit of 1 ppm were achieved. The LIG formation and electrochemical synthesis of PPy were confirmed through Raman spectroscopy and Fourier-transform infrared (FTIR) spectroscopy. The analysis by field emission scanning electron microscope (FE-SEM) and transmission electron microscopy (TEM) verified the formation of PPy@LIG NCs. In conclusion, this work introduces the novel PPy@LIG NCs and its application in gas sensing, showcasing their unique selectivity, enhanced sensitivity, and cost-effective production. These attributes mark a significant step forward, presenting new possibilities for the development of advanced gas-sensing systems aimed at improving air quality monitoring.**

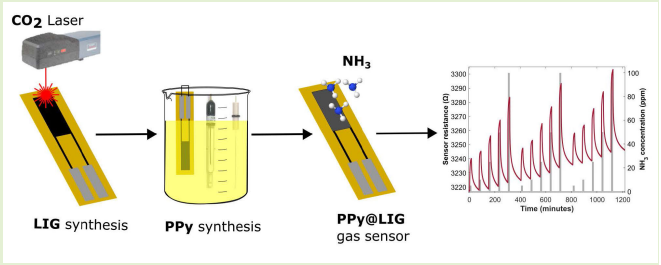

***Index Terms*— Ammonia (NH_3) sensor, chronoamperometry (CA), gas sensing, laser-induced graphene (LIG), polypyrrole (PPy).**

I. Introduction

IN MODERN society, gas measurements are essential in a wide range of applications, such as health, science, industry, environment, and technology. Among the gases of greatest interest, ammonia (NH_3) is a colorless species with a pungent, suffocating odor. It is emitted into the atmosphere from three principal sources. Two of these sources are natural processes: nitrification and ammonification, which result from the nitrogen cycle. An example of this cycle is the NH_3 emission resulting from livestock. The third source of NH_3 is combustion, from the chemical industry and motor vehicles [1].

The measurement of NH_3 is crucial in applications such as air quality monitoring [2], [3], regulation of agricultural and livestock practices [4], [5], [6], human breath analysis for medical applications [7], [8], and wastewater monitoring [9], [10]. In addition, the chemical industry produces NH_3 in large quantities to produce fertilizers and for use in refrigeration systems. Therefore, a gas leak in these industries could cause life-threatening situations [1], [11].

The U.S. National Institute for Occupational Safety and Health (NIOSH) defines threshold limit values (TLVs): a maximum 8-h time-weighted average (TWA) exposure to 25 ppm of NH_3, a short-term exposure limit (STEL) of 35 ppm in 15 min, and an immediately harmful to life or health (IDLH) of 300 ppm [12]. Extended exposure to elevated NH_3 concentrations can result in severe respiratory and central nervous system impairments [13], [14]. Due to the hazardous

Manuscript received 19 January 2024; accepted 19 February 2024. Date of publication 28 February 2024; date of current version 2 April 2024. This work was supported in part by the European Union (EU) in the Framework of H2020-MSCA-RISE-2018: Marie Sklodowska-Curie Actions under Grant 823895-PE, in part by the Ministerio de Ciencia, Innovación y Universidades (MICINN) under Grant PDC2022-133967-I00 and Grant TED2021-131442B-C31, and in part by the Agència de Gestió d'Ajuts Universitaris i de Recerca (AGAUR) under Grant 2021 SGR 00147. The work of José Carlos Santos-Ceballos was supported by the AGAUR-Personal Investigador Predoctoral en Formació (FI) ajuts Predoctoral Program (Joan Oró of the Secretariat of Universities and Research of the Department of Research and Universities of the Generalitat of Catalonia and the European Social Plus Fund) under Grant 2023 FI-2 00180. The work of Foad Salehnia was supported in part by the Spanish Ministry of Universities, Recovery, Transformation, and Resilience Plan, and in part by the Maria Zambrano Grant funded by the European Union—NextGenerationEU under Grant 2021URV-MZ-13. This is an expanded paper from the IEEE SENSORS 2023 Conference. The associate editor coordinating the review of this article and approving it for publication was Prof. Mahesh Kumar. *(Corresponding authors: Foad Salehnia; Xavier Vilanova.)*

The authors are with the MINOS Research Group, Department of Electronic, Electric and Automatic Engineering, School of Engineering, Universitat Rovira i Virgili, 43007 Tarragona, Spain (e-mail: josecarlos.santos@urv.cat; foad.salehnia@urv.cat; alfonsojose.romero@urv.cat; xavier.vilanova@urv.cat; eduard.llobet@urv.cat).

Digital Object Identifier 10.1109/JSEN.2024.3368658

nature of NH_3, it is essential to create sensitive sensors for real-time monitoring of this gas to ensure safety and identify potential risks.

The development of a flexible NH_3 sensor allows it to adapt to irregular and curved surfaces, and its light and thin profile makes it ideal for IoT applications and wearable devices [15]. Therefore, it can be used in a wide range of scenarios and surfaces, spanning from the clothing of a chemical industry worker to being placed on an animal on a farm.

In recent years, many researchers have developed numerous NH_3 sensors with different features such as new sensitive materials, structures, and fabrication methods. Among the most used approaches are optical [16], electrochemical [17], and chemoresistive gas sensors [18]. Although optical and electrochemical sensors show advantages in sensitivity, they show also some drawbacks, such as their high cost and complicated miniaturization [19].

For this reason, chemoresistive gas sensors, which employ films that undergo changes in resistance in the presence of a target gas, have attracted great attention, because of their numerous and unique characteristics, such as high sensitivity, ease of fabrication, simple operation, and low cost [20]. During the last decades, many research efforts have been focused on the development of NH_3 chemoresistive sensors based on metal oxides (MOXs) [21], [22], [23], which exhibit high gas sensitivity and rapid response and recovery dynamics, showing the potential for real-time monitoring applications. However, MOX-based sensors have some drawbacks such as the low selectivity to other gases. Usually, these sensors need high working temperatures, resulting in high power consumption and reduced durability of their gas detection properties [24].

Considering this, in recent years, attention has been diverted toward other chemoresistive materials that can work at room temperature, such as transition metal dichalcogenides (TMDs) [25] and graphene [26]. In particular, graphene-based sensors have attracted rising interest due to their unique molecular structure, high electrical conductivity and large surface area, high sensitivity to changes in gas concentration, and the potential for selective detection through chemical modification [27]. However, the commonly used graphene synthesis processes (chemical vapor deposition, micromechanical, chemical, and electrochemical exfoliation of graphite; thermal and chemical reduction of graphene oxide) [28] have challenges related to their high cost, difficulties for mass production, and integration into flexible electronic devices [29], [30].

In 2014, a one-step, simple, scalable, and low-cost approach was reported by Prof. Tour, for producing and patterning porous graphene films with 3-D networks from commercial polymer films, achieved using a CO_2 infrared laser [31]. This material is known as laser-induced graphene (LIG), which exhibits high porosity, excellent electrical conductivity, and good mechanical flexibility [32]. Also, LIG fibers show high thermal stability and outstanding electrochemical performance [33]. Due to their properties and facile laser fabrication process, it has been used in applications, including microfluidic systems, electronic devices, catalysis systems, water purification systems, and biosensors [34], [35].

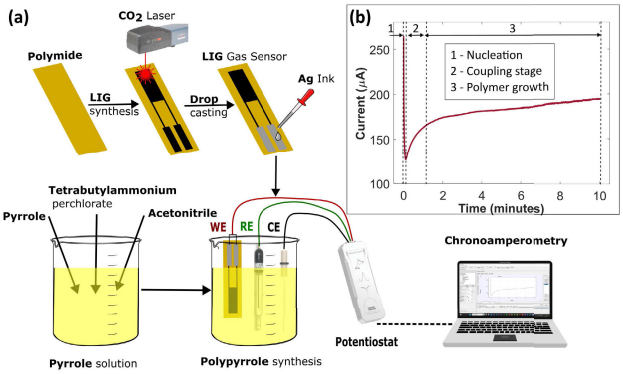

Fig. 1. Schematic illustration showing (a) fabrication process of the PPy@LIG NCs gas sensor and (b) chronoamperogram, describing the three steps of the electro-polymerization process for the electrodeposition on the LIG electrode.

Also, LIG has been used in gas-sensing applications, either as interdigitated electrodes [36], [37], [38], standalone sensitive layer [39], [40], or as composites with other nanomaterials such as MOX and TMD [41], [42], [43], [44]. These LIG composites provide the capability to identify multiple gas species. Nevertheless, LIG gas sensors for detecting NH_3 have been limited, due to the low response of LIG to this gas [37].

Recently, Casanova-Chafer et al. [45] used a graphene composite to increase the selectivity of their sensors to NH_3 gas. Commercial graphene was transformed into a composite by impregnation method with synthesized polypyrrole (PPy) nanoparticles. In our recent publication [46], this phenomenon was used as a starting point to develop an electrochemical approach to preparing flexible gas sensors with PPy@LIG nanocomposites (PPy@LIG NCs). To prepare the PPy nanocomposite, we used an electrochemical method to grow PPy on the LIG layer used as an electrode, instead of the impregnation method. The preliminary experimental results obtained in this work demonstrate that PPy improves the response of LIG to NH_3 operating at room temperature. Various electrochemical methods can be utilized for depositing PPy onto electrode surfaces. The commonly studied techniques include potentiodynamic approaches such as cyclic voltammetry (CV) or pulsed potential potentiostatic methods involving constant potential and time-dependent current variation [also known as chronoamperometry (CA)], and galvanostatic procedures employing constant current or current density over a specified period [also referred to as chronopotentiometry (CP)] [47], [48]. Starting from the promising results achieved, in this article, the different parameters of electrochemical deposition were fully explored to enhance this process and improve the response of the sensor to NH_3. Furthermore, a more complex study of the sensing properties of the sensor was carried out, which includes tests of repeatability, stability over time, performance under humid conditions, and selectivity toward other gases.

II. Experiment

A. Sensing Device Fabrication

The fabrication of the flexible gas sensor [Fig. 1(a)] involved two main steps. The first is fabricating a flexible LIG

electrode with the specific design of direct laser drawing. For this, a commercially available polyimide film (a thickness of 50 μm) glued to PET sheet was used as the flexible substrate. Initially, the substrate was cleaned with acetone. A CO_2 pulsed laser system (48-2, SYNRARD), with a wavelength of 10.6 μm and a max power of 25 W, was utilized for LIG synthesis. The laser was focused onto the polyimide surface using a lens with a focal length of 74 mm. The laser beam was then scanned over the substrate at a constant speed of 200 mm/s, a frequency of 12 kHz (a number of laser pulses per second), and a power level of 12%. These parameters are crucial in controlling the quality and characteristics of the resulting LIG, influencing its conductivity, morphology, and suitability for gas-sensing applications. To select the laser parameters, we used a simulation (Digital Twin) tool that we developed previously [49].

The LIG electrode has a sensing area of 3 × 6 mm and two square areas (contact pads) for the electrical connection with the measurement system. To improve electrical contact and stability of the sensor, Ag ink was drop-casted on these regions and allowed to dry at room temperature for 12 h. Following this step, the result is a 3-D porous graphene layer that provides us with whole sensing material, sensor connection, and electrodes altogether. The structure is schematized in Fig. 1(a).

In the second step, the electropolymerization of pyrrole was carried out using a potentiostat (pocketSTAT2, IVIUM Technologies). The process was conducted in an organic medium containing purified pyrrole monomer with a concentration of 0.25- and 0.5-mM tetrabutylammonium hexafluorophosphate (TBAPF6, Sigma-Aldrich, 99%) in acetonitrile as background electrolyte.

A three-electrode system comprised of bare LIG as working electrode, platinum wire auxiliary electrode, and Ag/AgCl reference electrode with salt bridge containing aqueous 3-M NaCl has been used in this process. In the following, the electrochemical polymerization of PPy was performed by applying a constant potential using CA. For achieving different sensors and optimizing the functionalization of LIG, the polymerization was conducted by applying different potentials to the LIG working electrode for different time durations and the resulting current was recorded as a function of time [$i = f(t)$]. This technique offers precise control over the electrochemical deposition process and has been widely utilized to design sensor materials.

The obtained chronoamperogram in Fig. 1(b) revealed a three-step mechanism, delineating the nucleation, coupling, and growth limitation stages during PPy formation. The nucleation stage, characteristic of conducting polymer formation, was marked by a rapid decrease in current density, indicative of radical cation formation, oxidative electroadsorption, and substrate passivation, occurring within a few seconds. Subsequently, the coupling stage exhibited a progressive increase in current density, representing the continuous and gradual growth of the conductive polymer. The final stage showed stabilization of current density, signaling growth limitation due to mass transfer reactions [50].

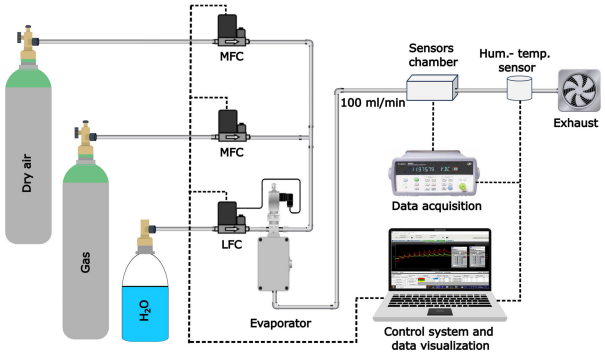

Fig. 2. Schematic illustration of gas measurement system used to evaluate the gas detection performance of manufactured sensors.

B. Characterization of the Gas-Sensitive Materials

The Raman analysis was conducted using a Renishaw InVia confocal Raman Spectrometer with coupled confocal microscope (Leica DM2500 Microsystems), employing two laser sources with different wavelengths (514 and 785 nm). The laser beam was focused onto the LIG surface through a 50× aperture objective lens, and the scattered light was collected and analyzed. The acquisition time was set to 30 s. For the detailed analysis of the structure of our hybrid material, transmission electron microscopy (TEM) was employed. The JEOL 1011 operated at 100 kV was used to conduct these examinations. A Scios 2 DualBeam field emission scanning electron microscope (FE-SEM) was used to analyze morphology. The JASCO FT/IR 6700 (Asia portal) spectrophotometer was employed for infrared spectroscopy analysis, providing detailed molecular information for the characterization.

C. Gas-Sensing Measurements

The gas-sensing characteristics of fabricated LIG gas sensors were assessed at room temperature (Fig. 2) within a sealed Teflon chamber, featuring a volume of 35 cm^3. This chamber is totally isolated from ambient humidity and has the capacity to measure four sensors at the same time. Then, the resistance of the different sensors was measured and recorded every 5 s using a data acquisition system (34972A LXI, Keysight) controlled with a PC application (BenchLink Data Logger 3, Agilent Technologies).

Different gas concentrations were applied by means of a mass-flow controller (MFC) system (EL-FLOW, Bronkhorst), controlled using PC applications (Flow View and Flow Plot, Bronkhorst). This system mixed the gases coming from a calibrated gas bottle with 100 ppm of NH_3 (balanced in dry air) and a bottle of dry, zero-grade air as the carrier. During all measurements, the total flow was kept at a constant low rate (100 mL/min) to work under more realistic experimental conditions. In addition, the gas-sensing performance of sensors under a humid atmosphere was characterized using a controller evaporator mixer (W-202A, Bronkhorst.) placed at the chamber's inlet. To monitor the actual environmental working conditions, a temperature and humidity sensor (SHT85, SENSIRION) was placed at the chamber outlet.

The sensors were stabilized under dry air for 90 min before exposure to repeated cycles of response (15 min) and recovery

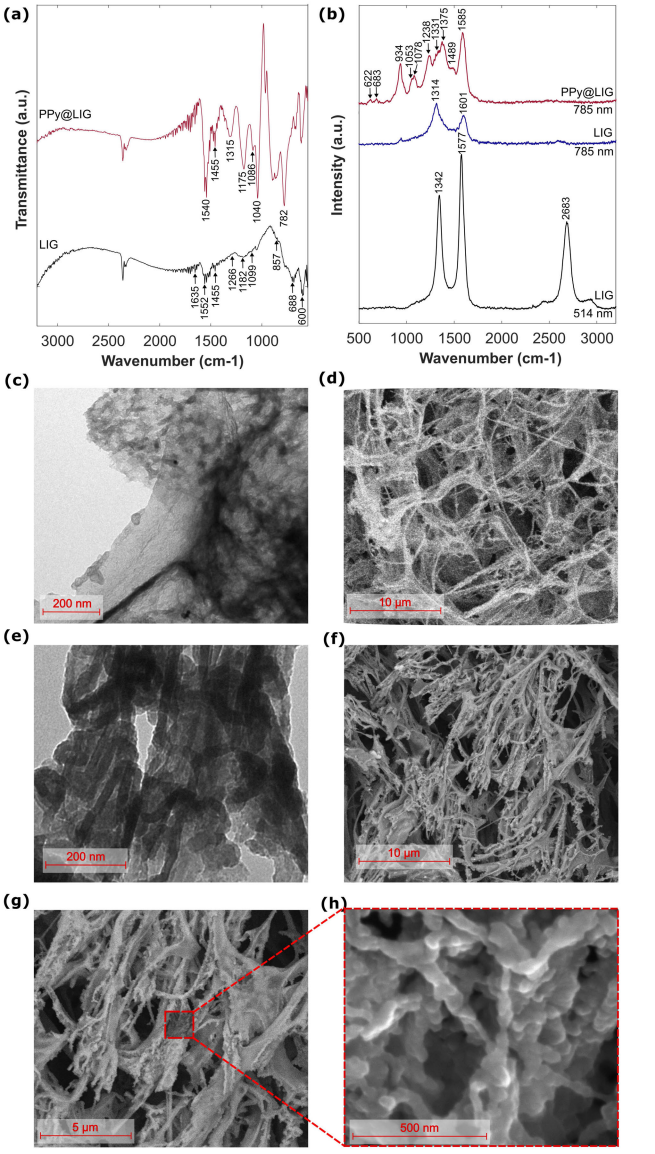

Fig. 3. Illustration showing (a) ATR-FTIR spectra of bare LIG and PPy@LIG NCs and (b) Raman spectra of bare LIG and PPy@LIG NCs. TEM images of (c) bare LIG and (e) PPy@LIG NCs. FE-SEM images of (d) bare LIG. (f)–(h) Different magnifications of PPy@LIG NC.

(60 min) to concentrations of 5, 10, 25, 50, and 100 ppm of NH_3 vapors. The sensor response was defined as $\Delta R/R_0$, expressed in percentage, where ΔR is the resistance changes recorded during exposure time to the target gas and R_0 is defined as the resistance of the sensor in dry air. To check the selectivity of the sensor to other gases, the same measurement system was employed, with the only variation of using a different gas bottle instead of the NH_3 bottle.

III. Results and Discussion

A. Structural and Morphological Studies

The attenuated total reflectance-Fourier-transform infrared (ATR-FTIR) spectra of LIG were examined and compared with the ATR-FTIR spectra of PPy role deposited on LIG (PPy@LIG) [Fig. 3(a)]. The FTIR spectrum for LIG displays characteristic peaks, with the prominent band at approximately 1635 cm^{t1}, signifying C=C stretching vibrations in the graphitic structure. Additional features in the LIG spectrum include peaks at around 1545–1552 and 1100 cm^{-1}, which are indicative of various in-plane vibrations and deformation modes. In the FTIR spectrum of PPy@LIG, new absorption bands are evident, confirming the successful integration of PPy with the LIG framework. The pronounced band at 1455 cm^{-1} is attributed to C–N stretching vibrations in the PPy, and the peaks near 1315 and 1040 cm^{-1} are likely associated with the in-plane bending of N–H and C–H in-plane deformation, respectively. The sharp absorption feature at 782 cm^{-1} could be ascribed to the out-of-plane C–H wagging in the PPy chains. The upper limit of 3200 cm^{-1} is chosen to accommodate the broad peaks associated with the hydroxyl (OH) groups, which extend beyond this range and may influence spectral interpretation [51].

The Raman spectra depicted in Fig. 3(b) offer a detailed look at the structural and vibrational properties of both LIG and PPy@LIG, highlighting the unique interaction between the two materials. For LIG, the *G*-band is observed around 1580 cm^{-1}, characteristic of sp^2-bonded carbon atoms in a hexagonal lattice, confirming the successful formation of graphene. This peak is indicative of the graphitic domains within the LIG. The *D*-band, located at approximately 1350 cm^{-1}, signifies the presence of defects and disorder in the graphene lattice, which is a common feature in LIG due to the rapid photothermal process of its formation. The ratio of the *D*-band to the *G*-band intensity (ID/IG) is a critical parameter in assessing the quality of graphene, with a higher ratio suggesting increased defects, which can be advantageous for certain applications where edge activity is beneficial [31], [32], [33].

Lin et al. [52] provide a comprehensive analysis of these structural features and their implications for the material's properties. The high degree of disorder in graphene can significantly impact its gas-sensing capabilities. Structural imperfections, such as vacancies, bond-angle disorder, and edge defects, influence the interaction between graphene and gas molecules. These defects can enhance the adsorption sites for gas molecules, potentially increasing the sensitivity of graphene-based gas sensors. Moreover, the specific nature of these defects can affect the selectivity of the sensor by altering the types of gas molecules preferentially adsorbed onto the graphene surface. In essence, the degree of disorder in graphene plays a crucial role in determining both the sensitivity and selectivity of graphene-based gas sensors.

The Raman spectra of PPy@LIG display characteristic peaks that align closely with the established literature values, allowing for minor shifts due to sample-specific factors. The spectrum reveals vibrational modes at 622 and 683 cm^{-1}, which are only slightly shifted from the expected positions, likely reflecting the sample's unique physical properties. A peak at 934 cm^{-1} indicates C–C ring deformation, hinting at the presence of charge carriers such as polarons or bipolarons. In the region associated with C–H in-plane deformation, peaks at 1053 and 1078 cm^{-1} are discerned, suggesting a slight alteration in the polymer chain's environment. The antisymmetric C–H in-plane bending mode is noted at 1232 cm^{-1}, closely corresponding to the literature value,

reinforcing the sample's structural integrity. Furthermore, the peaks at 1331 and 1375 cm^{-1} are attributed to the C–C in-ring and C–N stretching vibrations, with a minor red shift indicative of electronic structure consistency. At 1489 cm^{-1}, the vibrational mode associated with C–C and C=N stretching is observed, demonstrating a negligible deviation from the reference value. The peak at 1589 cm^{-1}, related to the C=C in-ring and C–C inter-ring stretching, confirms the polymer's conjugated structure. These observations suggest that the PPy nanoparticles retain their characteristic molecular vibrations with minor variations likely due to sample processing or instrumentation factors [53], [54].

Notably, the use of a 785-nm laser for Raman spectroscopy results in an enhanced signal from PPy with less interference from the LIG substrate. This can be attributed to the resonance Raman effect, where the laser excitation energy is closer to the electronic transitions of PPy, leading to an amplification of its Raman signal relative to that of LIG. This selective enhancement is beneficial for analyzing the PPy coatings on LIG, as it allows for clearer identification and analysis of the polymer's vibrational modes.

The TEM images in Fig. 3(c) and (e) provide a detailed visualization of the structure of the LIG and hybrid material, revealing the successful integration of PPy with the LIG.

In Fig. 3, a series of FE-SEM images provide valuable insights into the morphological characteristics of the fabricated materials. Fig. 3(d) presents the bare LIG, serving as the baseline for comparison. Fig. 3(f)–(h) showcases LIG modified with electro-deposited PPy at varying magnifications. In Fig. 3(f), a closer inspection reveals the intricate structure of LIG with PPy deposition, offering a detailed view of the interplay between graphene layers and the polymeric coating.

B. Sensing Performance Characterizations

To evaluate the sensing performance and impact of electrochemical deposition parameters on the sensing performance of the PPy@LIG sensors for NH_3 detection, various sensors were fabricated, and their responses were studied. Initially, with a constant deposition time of 10 min, the applied voltage to the system was set to different values (0.8, 1.0, 1.2, and 1.4 V). The obtained responses to different NH_3 concentrations and the resulting calibration curves are illustrated in Fig. 4(a). Further investigation revealed that at 0.8 V, only nucleation occurred during electropolymerization, leading to inadequate polymer growth and consequently suboptimal sensor response. At 1, 1.2, and 1.4 V, distinct polymer growth stages were observed. Notably, at 1 V, polymer growth was limited, while at 1.4 V, an excessive polymeric film formed, resulting in sensor response degradation due to film overload.

In addition, by varying the deposition time while maintaining a constant voltage (1.2 V), distinct growth characteristics were observed [Fig. 4(b)]. At 5 min, polymer growth was minimal, indicating insufficient development. Conversely, 15 and 20 min led to excessive growth, causing a reduction in sensor performance. The optimum balance between polymerization and sensor response was achieved at a deposition time of 10 min and a voltage of 1.2 V, resulting in a maximal intensity of resistance changes. This detailed exploration not

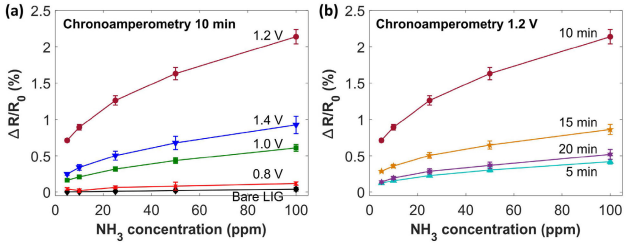

Fig. 4. Calibration curves of (a) bare LIG sensor and PPy@LIG NCs sensors manufactured with constant deposition time (10 min) and different voltages (0.8, 1.0, 1.2, and 1.4 V) and (b) PPy@LIG NCs sensors manufactured with different deposition times (5, 10, 15, and 20 min) and constant voltage (1.2 V).

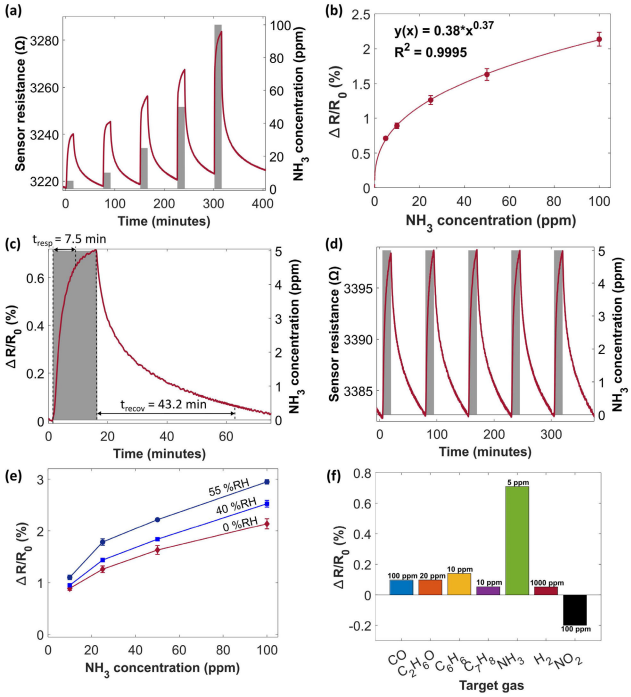

Fig. 5. Illustration showing the gas-sensing performance of the best PPy@LIG NCs gas sensors (1.2 V for 10 min). (a) Electrical response to different concentrations (5, 10, 25, 50, and 100 ppm) of NH_3 at room temperature. (b) Regression curve. (c) Response to 5 ppm of NH_3 and analysis of response/recovery time. (d) Electrical response to successive exposures of 5 ppm of NH_3. (e) Calibration curves obtained for different levels of humidity (0%RH, 40%RH, and 55%RH). (f) Response to different gas compounds (CO, C_2H_6O, C_6H_6, C_7H_8, NH_3, H_2, and NO_2).

only underscores the critical influence of electrochemical parameters on PPy@LIG sensor performance but also provides valuable insights for optimizing conditions to enhance NH_3 detection.

This sensor demonstrated responses up to 2.5 times greater compared to the sensor subjected to an electrochemical deposition time of 15 min. The enhanced performance can be attributed to the optimal balance achieved between polymerization and sensor response under these specific conditions. In Fig. 5(a), the dynamic electrical responses for the exemplary PPy@LIG gas sensors (1.2 V for 10 min) are illustrated, depicting increased resistance when exposed to varying concentrations of the target gas (NH_3). This heightened resistance arises from the diminished hole density and electrical conductivity of the p-type material (LIG) upon exposure to the

reducing gas, which acts as an electron donor. Moreover, the figures underscore the sensor's commendable baseline stability and minimal noise levels.

The regression analysis [Fig. 5(b)], depicting the sensor response modeled as a power function ($y(x) = 0.38x^{0.37}$) of concentration, provides a high correlation coefficient (R^2) of 0.9995. This R^2 value suggests that the power function adequately describes the gas concentration and sensor response relationship.

To determine the limit of detection (LOD), a methodical approach aligned with the IUPAC definition was employed [55]. The IUPAC has recommended that the LOD, defined in terms of concentration, is related to the smallest measure of response (x_L) that can be detected with reasonable certainty in a given analytical procedure in the following equation:

$$x_L = \bar{x}_B + ks_B \tag{1}$$

where $\bar{x}_B$ is the mean of the blank measures, s_B is the standard deviation of the blank measures, and k is a numerical factor chosen according to the confidence level desired (a value of $k = 3$ is recommended). The detection limit is given by the following equation:

$$\text{LOD} = ks_B/S \tag{2}$$

where S is the sensitivity (slope) derived from the calibration curve. Following this methodology, the PPy@LIG sensor exhibits an LOD of 1000 ppb for NH_3. This sensitivity places it on par with other varieties of organic-based nanomaterials, underscoring its potential efficacy in gas detection applications.

The response time (t_{resp}) and recovery time (t_{recov}) are calculated as the time to reach 90% of total resistance change for NH_3 exposure and air re-exposure, respectively. In the case of the sensor response to 5 ppm of NH_3 [Fig. 5(c)], the calculated $t_{\text{resp}}/t_{\text{recov}}$ values are 7.5/43.2 min. Considering that this concentration is below the TLV defined by NIOSH and no fast detectors are required, a response time in the order of minutes is sufficient. It can be concluded that these times are adequate for this sensor to be used in NH_3 real-time monitoring in the environment.

In regard to the response and recovery times, as well as the drift issue in Fig. 5(a), our research acknowledges that the integration of a heater might improve these aspects. However, the core innovation of our study is the development of a sensor that functions efficiently at room temperature without the need for additional heating elements. This design emphasizes the sensor's simplicity and energy efficiency, key factors for its practical application in real-world scenarios.

Moreover, an insightful observation from Table I reveals that the response time diminishes with an escalation in NH_3 concentration, while the recovery time experiences an increase. In gas-sensing systems, the response time typically involves two primary processes: the diffusion of gas molecules to the sensor surface and the subsequent chemical reaction or adsorption occurring at the sensing material. As the concentration of NH_3 increases, the number of gas molecules available for diffusion also rises. In scenarios where the gas concentration is relatively low, the diffusion process becomes the predominant factor influencing response time. For concentrations such as 100 ppm, where the response time is notably low (5.33 min), this suggests that the sensor's ability to detect NH_3 at higher concentrations is primarily hindered by the diffusion of gas molecules to the sensor surface rather than the chemical reaction kinetics.

TABLE I
RESPONSE AND RECOVERY TIMES OF PPY@LIG GAS SENSORS (1.2 V FOR 10 MIN)

NH_3 concentration (ppm)	Response time (min)	Recovery time (min)
5	7.75	43.20
10	7.06	44.57
25	6.75	45.21
50	6.42	45.52
100	5.33	46.25

At higher concentrations, the gas molecules are more abundant and readily reach the sensor's active sites, leading to a faster response time. Conversely, the observed increase in recovery time at higher concentrations could be attributed to the persistence of gas molecules within the sensor matrix, necessitating a longer duration for complete desorption or clearance during air re-exposure.

The sensor repeatability was evaluated by applying successive NH_3 pulses for 15 min and recovery steps of 60 min between gas exposures. Fig. 5(d) shows excellent sensor repeatability, in which the hybrid nanomaterial PPy@LIG presents an error of about 1.34%. However, it is noteworthy to mention that during our measurements, a small constant drift was detected in the readings. This drift, while present, has been deliberately omitted from the presented graph to ensure clarity and focus on the sensor's inherent repeatability characteristics.

Investigation into the impact of environmental moisture on gas sensor performance has highlighted humidity as a crucial factor that significantly alters sensor response. An experiment was conducted under varying humidity levels to evaluate this effect and compared the results with those obtained under dry conditions. The data presented in Fig. 5(e) clearly show that sensor response to NH_3 is dependent on the relative humidity (RH) of the environment. At 55% RH, the sensor's response was higher than at 40%RH and 0%RH across all tested NH_3 concentrations. Specifically, at 55%RH, the sensor response for 100 ppm was elevated, indicating an increase in sensitivity compared to lower humidity levels. This trend suggests that the presence of moisture facilitates the adsorption of NH_3 molecules, potentially due to a swelling effect within the sensor's active material, which increases the spacing between conductive domains and, thus, the overall resistance. In addition, the moist environment may promote a more effective proton exchange with NH_3, further amplifying the sensor's resistance changes. These findings substantiate the need to integrate humidity considerations into deploying NH_3 sensors to ensure accurate and reliable performance in varying atmospheric conditions.

Furthermore, selectivity was assessed [Fig. 5(f)] by measuring high concentrations of other reducing species, including

TABLE II
SUMMARY OF RECENT RESEARCH RESULTS FOR NH_3 SENSORS

Sensing material	Fabrication method	Sensitivity (%/ppm)	LOD (ppm)	T_{resp}/T_{recov} (sec)	Flex	Ref.
PEDOT: Pss/G	Electronic ink	9.6/500	25	180/300	Yes	[56]
MXene	Coating on ceramic	6/500	10	45/94	No	[57]
ZnO/CuO @G	Hydrothermal growth	4.9/5	-	4.1/2	Yes	[58]
Gr/Ag–Ag2O/PPy	In-situ polymerization	9.26/1000	150	40/60	No	[59]
PPy+MW CNT	Chemical Oxidation	3.07/200	-	34/180	No	[60]
PPy NW	Electro polymerization	0.06/1	40	900/-	No	[61]
PPy+G (CVD)	Electro polymerization	1.7/1		120/300	No	[62]
PPy@G	Chemical polymerization	0.88/1	0.419	300/900	No	[45]
PPy@LIG	Electro polymerization	2.13/100	1	318/2775	Yes	This work

100 ppm of carbon monoxide (CO), 100 ppm of hydrogen (H_2), 20 ppm of ethanol (C_2H_6O), and aromatic volatile organic compounds (VOCs) such as 10 ppm of benzene (C_6H_6) and 10 ppm of toluene (C_7H_8). In addition, the sensor was exposed to an oxidizing gas, 100 ppm of nitrogen dioxide (NO_2), which is one of the most present polluting gases in the atmosphere. As a result, lower responses were obtained toward these analytes in comparison to 5 ppm of NH_3, making the PPy@LIG gas sensor reliable and promising to detect NH_3 in the environment.

Table II outlines various NH_3 gas sensors, emphasizing performance in sensitivity, detection limits, response times, and flexibility. Our research introduces a sensor with a practical balance of effectiveness and utility. Our sensor's sensitivity is 2.13% per 100 ppm, and although not the highest, it shows the low LOD at 1 ppm, showcasing its ability to detect low NH_3 levels. The response times are moderate at 318/2775 s, making it suitable for real-world use. A standout feature of our sensor is its cost-effectiveness and reproducibility, which are essential for widespread use. The chosen manufacturing process, electro-polymerization, is economically advantageous and produces consistent sensor layers, vital for reliable readings. In addition, our sensor is flexible in operation. This sensor marks a significant leap in gas-sensing technology, presenting an economical and consistent option compared to other sensors.

C. Gas-Sensing Mechanism and the Advantages of LIG

When the sensitive layer engages with electron-donating molecules such as NH_3, a reduction in hole density occurs, resulting in an increase in electrical resistance. Experimental findings suggest that bare graphene exhibits interaction with NH_3 molecules; however, the incorporation of PPy on the LIG amplifies this interaction significantly. In essence, the coexistence of LIG and PPy engenders a synergistic sensing effect, wherein both nanomaterials collaboratively interact with the target gas, yielding heightened sensing performance. Moreover, the noteworthy interaction observed between the two nanomaterials is facilitated by robust hydrogen bonds and $\pi - \pi$-stacking. This interaction not only contributes to long-term sensor stability but also enhances the efficiency of gas sensing. In addition, the substantial surface area of graphene and its superior electron mobility facilitate rapid and efficient charge transfer with PPy@LIG, resulting in an effective transduction process.

LIG emerges as a superior sensing material due to its distinctive properties, such as high porosity, exceptional electrical conductivity, and robust mechanical flexibility, making it especially suitable for gas detection applications. The fabrication process of LIG, involving a direct writing method using a CO_2 laser on polyimide sheets, is both cost-effective and scalable. This technique simplifies the production process and allows for precise patterning, enhancing the material's applicability. Furthermore, LIG's compatibility with various nanomaterials, such as MOXs, significantly broadens its utility across a range of sensing applications. In this study, we leverage these unique attributes of LIG, particularly focusing on its application in developing efficient NH_3 sensors, thereby demonstrating its potential in environmental monitoring and safety applications.

IV. CONCLUSION

In conclusion, this study is focused on the electrochemical synthesis of PPy on LIG electrodes and explored the gas-sensing applications of the resulting PPy@LIG NCs, with a specific emphasis on detecting NH_3 at room temperature. The proposed simple and scalable method for the low-cost, large-scale production of PPy@LIG NCs proved effective, demonstrating promising attributes for gas-sensing applications. The investigation into the sensing performance of the PPy@LIG sensors for NH_3 detection provided valuable insights into the impact of electrochemical deposition parameters. Through systematic variations in deposition time and applied voltage, it was revealed that an optimal balance between polymerization and sensor response was achieved at a deposition time of 10 min and a voltage of 1.2 V. This specific set of conditions resulted in a maximal intensity of resistance changes and significantly enhanced sensor responses compared to other parameter combinations. The dynamic responses of the PPy@LIG gas sensors illustrated commendable baseline stability, minimal noise levels, and increased resistance when exposed to varying concentrations of NH_3. Regression analysis demonstrated a high correlation coefficient (R^2) of 0.9995, indicating that the power function adequately described the relationship between gas concentration and sensor response. Furthermore, the calculated response time and recovery time for the sensor's response to 5 ppm of NH_3 were found to be 7.5 and 43.2 min, respectively. Considering that this concentration is below the TLV defined by NIOSH and no fast detectors are required, these response times were deemed sufficient for real-time monitoring of NH_3 in the environment. In summary, the PPy@LIG nanocomposites exhibited excellent sensitivity, repeatability, and a low detection limit, showcasing their potential for application in gas-sensing networks tailored for air quality monitoring. The detailed exploration of electrochemical parameters not only emphasized their critical influence on sensor performance but also provided valuable guidance for optimizing conditions to

enhance NH_3 detection. The results presented in this article contribute to the advancement of flexible and cost-effective gas sensors with potential applications in environmental monitoring and beyond.

REFERENCES

[1] B. Timmer, W. Olthuis, and A. V. D. Berg, "Ammonia sensors and their applications—A review," *Sens. Actuators B, Chem.*, vol. 107, no. 2, pp. 666–677, Jun. 2005, doi: 10.1016/j.snb.2004.11.054.

[2] W. Wang, S. Wang, J. Xu, R. Zhou, C. Shi, and B. Zhou, "Gas-phase ammonia and $PM_{2.5}$ ammonium in a busy traffic area of Nanjing, China," *Environ. Sci. Pollut. Res.*, vol. 23, no. 2, pp. 1691–1702, Jan. 2016, doi: 10.1007/s11356-015-5397-3.

[3] A. A. Nair and F. Yu, "Quantification of atmospheric ammonia concentrations: A review of its measurement and modeling," *Atmosphere*, vol. 11, no. 10, p. 1092, Oct. 2020, doi: 10.3390/atmos11101092.

[4] M. Insausti, R. Timmis, R. Kinnersley, and M. C. Rufino, "Advances in sensing ammonia from agricultural sources," *Sci. Total Environ.*, vol. 706, Mar. 2020, Art. no. 135124, doi: 10.1016/j.scitotenv.2019.135124.

[5] J. Liu et al., "Highly efficient reduction of ammonia emissions from livestock waste by the synergy of novel manure acidification and inhibition of ureolytic bacteria," *Environ. Int.*, vol. 172, Feb. 2023, Art. no. 107768, doi: 10.1016/j.envint.2023.107768.

[6] F. K. Shaikh, S. Karim, S. Zeadally, and J. Nebhen, "Recent trends in Internet-of-Things-enabled sensor technologies for smart agriculture," *IEEE Internet Things J.*, vol. 9, no. 23, pp. 23583–23598, Dec. 2022, doi: 10.1109/JIOT.2022.3210154.

[7] M. J. Lefferts and M. R. Castell, "Ammonia breath analysis," *Sensors Diag.*, vol. 1, no. 5, pp. 955–967, Sep. 2022, doi: 10.1039/d2sd00089j.

[8] A. Abbaszadeh, S. Makouei, and S. Meshgini, "Ammonia measurement in exhaled human breath using PCF sensor for medical applications," *Photon. Nanostruct.-Fundamentals Appl.*, vol. 44, May 2021, Art. no. 100917, doi: 10.1016/j.photonics.2021.100917.

[9] X. Fang, X. Guo, H. Shi, and Q. Cai, "Determination of ammonia nitrogen in wastewater using electronic nose," in *Proc. 4th Int. Conf. Bioinf. Biomed. Eng.*, Jun. 2010, pp. 1–4, doi: 10.1109/ICBBE.2010.5515426.

[10] V. Blanes-Vidal, M. Guardia, X. R. Dai, and E. S. Nadimi, "Emissions of NH_3, CO_2 and H_2S during swine wastewater management: Characterization of transient emissions after air-liquid interface disturbances," *Atmos. Environ.*, vol. 54, pp. 408–418, Jul. 2012, doi: 10.1016/j.atmosenv.2012.02.046.

[11] R. Yuliarti, K. Khambali, and R. Rusmiati, "Risk analysis of exposure to NH_3 and H_2S gas to workers in the small industrial environment of magetan regency in 2021," *Int. J. Adv. Health Sci. Technol.*, vol. 2, no. 3, pp. 169–174, Jun. 2022, doi: 10.35882/ijahst.v2i3.7.

[12] *CDC—NIOSH Pocket Guide to Chemical Hazards—Ammonia*. Accessed: Nov. 7, 2023. [Online]. Available: https://www.cdc.gov/niosh/npg/npgd0028.html

[13] A. Adlimoghaddam, M. G. Sabbir, and B. C. Albensi, "Ammonia as a potential neurotoxic factor in Alzheimer's disease," *Front Mol Neurosci*, vol. 9, Aug. 2016, Art. no. 209776, doi: 10.3389/fnmol.2016.00057.

[14] M. Li, C. J. Weschler, G. Bekö, P. Wargocki, G. Lucic, and J. Williams, "Human ammonia emission rates under various indoor environmental conditions," *Environ. Sci. Technol.*, vol. 54, no. 9, pp. 5419–5428, May 2020, doi: 10.1021/acs.est.0c00094.

[15] U. Choudhari and S. Jagtap, "A panoramic view of NO_x and NH_3 gas sensors," *Nano-Struct. Nano-Objects*, vol. 35, Jul. 2023, Art. no. 100995, doi: 10.1016/j.nanoso.2023.100995.

[16] A. Hadi Ismail and Y. Sulaiman, "Review on the utilisation of sensing materials for intrinsic optical NH_3 gas sensors," *Synth. Met.*, vol. 280, Oct. 2021, Art. no. 116860, doi: 10.1016/j.synthmet.2021.116860.

[17] S. Nithya and A. Dutta, "Superior dual mode electrochemical sensing of NH_3 using Ni^{2+} doped CuO anode with lanthanum gallate based electrolyte," *Sens. Actuators B, Chem.*, vol. 361, Jun. 2022, Art. no. 131731, doi: 10.1016/j.snb.2022.131731.

[18] D. Kwak, Y. Lei, and R. Maric, "Ammonia gas sensors: A comprehensive review," *Talanta*, vol. 204, pp. 713–730, Nov. 2019, doi: 10.1016/j.talanta.2019.06.034.

[19] Z. Bielecki, T. Stacewicz, J. Smulko, and J. Wojtas, "Ammonia gas sensors: Comparison of solid-state and optical methods," *Appl. Sci.*, vol. 10, no. 15, p. 5111, Jul. 2020, doi: 10.3390/app10155111.

[20] S. M. Majhi, A. Mirzaei, H. W. Kim, S. S. Kim, and T. W. Kim, "Recent advances in energy-saving chemiresistive gas sensors: A review," *Nano Energy*, vol. 79, Jan. 2021, Art. no. 105369, doi: 10.1016/j.nanoen.2020.105369.

[21] A. Dey, "Semiconductor metal oxide gas sensors: A review," *Mater. Sci. Eng., B*, vol. 229, pp. 206–217, Mar. 2018, doi: 10.1016/j.mseb.2017.12.036.

[22] N. Van Duy et al., "Enhancement of NH_3 gas sensing with Ag-Pt co-catalyst on SnO_2 nanofilm towards medical diagnosis," *Thin Solid Films*, vol. 767, Feb. 2023, Art. no. 139682, doi: 10.1016/j.tsf.2023.139682.

[23] S. S. Shetty, A. Jayarama, S. Bhat, I. Karunasagar, and R. Pinto, "A review on metal-oxide based trace ammonia sensor for detection of renal disease by exhaled breath analysis," *Mater. Today, Proc.*, vol. 55, pp. 113–117, Jan. 2022, doi: 10.1016/j.matpr.2021.12.411.

[24] C. Wang, L. Yin, L. Zhang, D. Xiang, and R. Gao, "Metal oxide gas sensors: Sensitivity and influencing factors," *Sensors*, vol. 10, no. 3, pp. 2088–2106, 2010, doi: 10.3390/s100302088.

[25] P. Goswami and G. Gupta, "Recent progress of flexible NO_2 and NH_3 gas sensors based on transition metal dichalcogenides for room temperature sensing," *Mater. Today Chem.*, vol. 23, Mar. 2022, Art. no. 100726, doi: 10.1016/j.mtchem.2021.100726.

[26] X. Tang, M. Debliquy, D. Lahem, Y. Yan, and J.-P. Raskin, "A review on functionalized graphene sensors for detection of ammonia," *Sensors*, vol. 21, no. 4, p. 1443, Feb. 2021, doi: 10.3390/s21041443.

[27] M. Hao, W. Zeng, Y.-Q. Li, and Z.-C. Wang, "Three-dimensional graphene and its composite for gas sensors," *Rare Met.*, vol. 40, no. 6, pp. 1494–1514, Jun. 2021, doi: 10.1007/s12598-020-01633-9.

[28] K. E. Whitener and P. E. Sheehan, "Graphene synthesis," *Diamond Rel. Mater.*, vol. 46, pp. 25–34, Jun. 2014, doi: 10.1016/j.diamond.2014.04.006.

[29] F. Liu, P. Li, H. An, P. Peng, B. McLean, and F. Ding, "Achievements and challenges of graphene chemical vapor deposition growth," *Adv. Funct. Mater.*, vol. 32, no. 42, Oct. 2022, Art. no. 2203191, doi: 10.1002/adfm.202203191.

[30] L. Lin, H. Peng, and Z. Liu, "Synthesis challenges for graphene industry," *Nature Mater.*, vol. 18, no. 6, pp. 520–524, Jun. 2019, doi: 10.1038/s41563-019-0341-4.

[31] J. Lin et al., "Laser-induced porous graphene films from commercial polymers," *Nature Commun.*, vol. 5, p. 5714, Dec. 2014, doi: 10.1038/NCOMMS6714.

[32] R. Ye, D. K. James, and J. M. Tour, "Laser-induced graphene," *Accounts Chem. Res.*, vol. 51, no. 7, pp. 1609–1620, Jul. 2018, doi: 10.1021/acs.accounts.8b00084.

[33] L. X. Duy, Z. Peng, Y. Li, J. Zhang, Y. Ji, and J. M. Tour, "Laser-induced graphene fibers," *Carbon*, vol. 126, pp. 472–479, Jan. 2018, doi: 10.1016/j.carbon.2017.10.036.

[34] F. M. Vivaldi et al., "Three-dimensional (3D) laser-induced graphene: Structure, properties, and application to chemical sensing," *ACS Appl. Mater. Interfaces*, vol. 13, no. 26, pp. 30245–30260, Jul. 2021, doi: 10.1021/acsami.1c05614.

[35] L. Cheng et al., "Laser-induced graphene for environmental applications: Progress and opportunities," *Mater. Chem. Frontiers*, vol. 5, no. 13, pp. 4874–4891, 2021, doi: 10.1039/D1QM00437A.

[36] W. Yan, W. Yan, T. Chen, J. Xu, Q. Tian, and D. Ho, "Size-tunable flowerlike MoS_2 nanospheres combined with laser-induced graphene electrodes for NO_2 sensing," *ACS Appl. Nano Mater.*, vol. 3, no. 3, pp. 2545–2553, Mar. 2020, doi: 10.1021/acsanm.9b02614.

[37] Z. Peng et al., "A multi-functional NO_2 gas monitor and self-alarm based on laser-induced graphene," *Chem. Eng. J.*, vol. 428, Jan. 2022, Art. no. 131079, doi: 10.1016/j.cej.2021.131079.

[38] S.-F. Tseng, P.-S. Chen, S.-H. Hsu, W.-T. Hsiao, and W.-J. Peng, "Investigation of fiber laser-induced porous graphene electrodes in controlled atmospheres for ZnO nanorod-based NO_2 gas sensors," *Appl. Surf. Sci.*, vol. 620, May 2023, Art. no. 156847, doi: 10.1016/j.apsusc.2023.156847.

[39] M. G. Stanford, K. Yang, Y. Chyan, C. Kittrell, and J. M. Tour, "Laser-induced graphene for flexible and embeddable gas sensors," *ACS Nano*, vol. 13, no. 3, pp. 3474–3482, 2019, doi: 10.1021/acsnano.8b09622.

[40] L. Yang et al., "Moisture-resistant, stretchable NO_x gas sensors based on laser-induced graphene for environmental monitoring and breath analysis," *Microsyst. Nanoeng.*, vol. 8, no. 1, p. 78, Jul. 2022, doi: 10.1038/s41378-022-00414-x.

[41] J. Zhao et al., "In situ laser-assisted synthesis and patterning of graphene foam composites as a flexible gas sensing platform," *Chem. Eng. J.*, vol. 456, Jan. 2023, Art. no. 140956, doi: 10.1016/j.cej.2022.140956.

[42] L. Yang et al., "Novel gas sensing platform based on a stretchable laser-induced graphene pattern with self-heating capabilities," *J. Mater. Chem. A*, vol. 8, no. 14, pp. 6487–6500, Apr. 2020, doi: 10.1039/c9ta07855j.
[43] N. Yi et al., "Stretchable, ultrasensitive, and low-temperature NO_2 sensors based on MoS_2@rGO nanocomposites," *Mater. Today Phys.*, vol. 15, Dec. 2020, Art. no. 100265, doi: 10.1016/j.mtphys.2020.100265.
[44] L. Yang et al., "Intrinsically breathable and flexible NO_2 gas sensors produced by laser direct writing of self-assembled block copolymers," *ACS Appl. Mater. Interfaces*, vol. 14, no. 15, pp. 17818–17825, Apr. 2022, doi: 10.1021/acsami.2c02061.
[45] J. Casanova-Chafer, P. Umek, S. Acosta, C. Bittencourt, and E. Llobet, "Graphene loading with polypyrrole nanoparticles for trace-level detection of ammonia at room temperature," *ACS Appl. Mater. Interfaces*, vol. 13, no. 34, pp. 40909–40921, Sep. 2021, doi: 10.1021/acsami.1c10559.
[46] J. C. Santos-Ceballos, F. Salehnia, A. Romero, and X. Vilanova, "Flexible sensor utilizing polypyrrole laser-induced graphene nanocomposite for room temperature ammonia detection," in *Proc. IEEE SENSORS*, Oct. 2023, pp. 1–4, doi: 10.1109/sensors56945.2023.10325068.
[47] E. Sobhanie, M. Hosseini, F. Faridbod, and M. R. Ganjali, "Sensitive detection of H_2O_2 released from cancer cells with electrochemiluminescence sensor based on electrochemically prepared polypyrrole@ce: Dy tungstate/polyluminol," *J. Electroanal. Chem.*, vol. 932, Mar. 2023, Art. no. 117244, doi: 10.1016/j.jelechem.2023.117244.
[48] A. Karimi, S. W. Husain, M. Hosseini, P. A. Azar, and M. R. Ganjali, "A sensitive signal-on electrochemiluminescence sensor based on a nanocomposite of polypyrrole-Gd_2O_2 for the determination of L-cysteine in biological fluids," *Microchimica Acta*, vol. 187, no. 7, p. 398, Jul. 2020, doi: 10.1007/s00604-020-04372-x.
[49] J. C. Santos-Ceballos, F. Salehnia, A. Romero, and X. Vilanova, "Leveraging digital twins for optimized fabrication: Simulation-based enhancement of laser-induced graphene writing," unpublished.
[50] M. Lo et al., "Polypyrrole: A reactive and functional conductive polymer for the selective electrochemical detection of heavy metals in water," *Emergent Mater.*, vol. 3, no. 6, pp. 815–839, Dec. 2020, doi: 10.1007/s42247-020-00119-9.
[51] J. Tabaciarová, M. Micusík, P. Fedorko, and M. Omastová, "Study of polypyrrole aging by XPS, FTIR and conductivity measurements," *Polym. Degradation Stability*, vol. 120, pp. 392–401, Oct. 2015, doi: 10.1016/j.polymdegradstab.2015.07.021.
[52] Z. Lin, L. Ji, T. Yan, Y. Xu, and Z. Sun, "Surface defects state analysis of laser induced graphene from 4H-SiC," *J. Mater. Res. Technol.*, vol. 9, no. 3, pp. 5934–5941, May 2020, doi: 10.1016/j.jmrt.2020.03.120.
[53] M. Setka, R. Calavia, L. Vojkuvka, E. Llobet, J. Drbohlavová, and S. Vallejos, "Raman and XPS studies of ammonia sensitive polypyrrole nanorods and nanoparticles," *Sci. Rep.*, vol. 9, no. 1, p. 8465, Jun. 2019, doi: 10.1038/s41598-019-44900-1.
[54] M. Trchová and J. Stejskal, "Resonance Raman spectroscopy of conducting polypyrrole nanotubes: Disordered surface versus ordered body," *J. Phys. Chem. A*, vol. 122, no. 48, pp. 9298–9306, Dec. 2018, doi: 10.1021/acs.jpca.8b09794.
[55] Analytical Methods Committee, "Recommendations for the definition, estimation and use of the detection limit," *Analyst*, vol. 112, no. 2, pp. 199–204, Jan. 1987, doi: 10.1039/AN9871200199.
[56] Y. Seekaew, S. Lokavee, D. Phokharatkul, A. Wisitsoraat, T. Kerdcharoen, and C. Wongchoosuk, "Low-cost and flexible printed graphene-PEDOT:PSS gas sensor for ammonia detection," *Organic Electron.*, vol. 15, no. 11, pp. 2971–2981, Nov. 2014, doi: 10.1016/j.orgel.2014.08.044.
[57] M. Wu et al., "Ti_3C_2 MXene-based sensors with high selectivity for NH_3 detection at room temperature," *ACS Sensors*, vol. 4, no. 10, pp. 2763–2770, Oct. 2019, doi: 10.1021/acssensors.9b01308.
[58] M. Jagannathan, D. Dhinasekaran, A. R. Rajendran, and B. Subramaniam, "Selective room temperature ammonia gas sensor using nanostructured ZnO/CuO@graphene on paper substrate," *Sens. Actuators B, Chem.*, vol. 350, Jan. 2022, Art. no. 130833, doi: 10.1016/j.snb.2021.130833.
[59] M. Shoeb, M. Mobin, S. Ahmad, and A. H. Naqvi, "Facile synthesis of polypyrrole coated graphene Gr/Ag–Ag_2O/PPy nanocomposites for a rapid and selective response towards ammonia sensing at room temperature," *J. Sci., Adv. Mater. Devices*, vol. 6, no. 2, pp. 223–233, Jun. 2021, doi: 10.1016/j.jsamd.2021.02.003.
[60] S. G. Bachhav and D. R. Patil, "Study of polypyrrole-coated MWCNT nanocomposites for ammonia sensing at room temperature," *J. Mater. Sci. Chem. Eng.*, vol. 3, no. 10, pp. 30–44, Oct. 2015, doi: 10.4236/msce.2015.310005.
[61] M. Setka, J. Drbohlavová, and J. Hubálek, "Nanostructured polypyrrole-based ammonia and volatile organic compound sensors," *Sensors*, vol. 17, no. 3, p. 562, Mar. 2017, doi: 10.3390/s17030562.
[62] X. Tang et al., "A fast and room-temperature operation ammonia sensor based on compound of graphene with polypyrrole," *IEEE Sensors J.*, vol. 18, no. 22, pp. 9088–9096, Nov. 2018, doi: 10.1109/JSEN.2018.2869203.

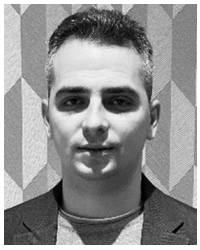

José Carlos Santos-Ceballos received the B.S. degree in automatic engineering and the M.S. degree in digital system from the Universidad Tecnológica de La Habana "José Antonio Echeverría," (CUJAE), Havana, La Habana, Cuba, in 2015 and 2020, respectively. He is pursuing the Ph.D. degree with the Department of Electronic, Electrical and Automatic Control Engineering, Universitat Rovira i Virgili, Tarragona, Spain.

From 2015 to 2022, he was an Electronic Design Specialist with the Development Department, Cuban Center for Neuroscience, Havana, La Habana, Cuba. His research interests include wearable gas sensors, signal processing for gas sensing, and embedded systems.

Foad Salehnia was born in Sanandaj, Iran. He received the Ph.D. degree in nanochemistry from the University of Tehran, Tehran, Iran, in 2019.

He subsequently pursued two postdoctoral positions with the University of Tehran. He is a Maria Zambrano Research Fellow with the MINOS Research Group, Universitat Rovira i Virgili, Tarragona, Spain. His research interests include synthesizing novel carbon-based nanomaterials and investigating their applications in sensing areas and energy conversion systems.

Alfonso Romero received the Ph.D. degree from the Universitat Politècnica de Catalunya (UPC) Barcelona, Spain, in 2001.

He is an Associate Professor in Electronics Technology with the Universitat Rovira i Virgili, Tarragona, Spain. His research interests include instrumentation electronics applied to electronic sensors measurements and data transmissions.

Xavier Vilanova received the Ph.D. degree from the Universitat Politècnica de Catalunya (UPC), Barcelona, Spain, in 1998. Since 2010, he has been a Full Professor of Electronics Technology with the Universitat Rovira i Virgili, Tarragona, Spain. His research interests include gaining insight into the information extracted from gas sensor transients when exposed to pulsed light excitation. He is also working on developing scalable and low-cost processes to obtain flexible gas sensors.

Eduard Llobet (Senior Member, IEEE) received the Ph.D. degree from the Universitat Politècnica de Catalunya (UPC), Barcelona, Spain, in 1997.

He was a Postdoctoral Researcher with the University of Warwick, Coventry, U.K., for one year. He is a Full Professor of Electronics with the Universitat Rovira i Virgili, Tarragona, Spain. His research interests include gaining insight in surface chemistry, nature of defects, and the specific mechanisms of the interaction of metal oxides, transition metal dichalcogenides, and carbon nanomaterials with target gases, unveiling gas-sensing mechanisms, and structure–performance relationships. He is also working toward the realization of nanomaterial-based flexible gas sensors and sensor systems with a performance that matches the one of conventional rigid devices.